Journal of Dental Research
2017, Vol. 96(7) 798–806

DOI: 10.1177/0022034517695496
journals.sagepub.com/home/jdr

L1 Peptide–Conjugated Fibrin Hydrogels Promote Salivary Gland Regeneration

K. Nam[1], C.-S. Wang[1], C.L.M. Maruyama[1], P. Lei[2], S.T. Andreadis[2,3,4], and O.J. Baker[1]

Abstract

Hyposalivation contributes to dental caries, periodontitis, and microbial infections. Additionally, it impairs activities of daily living (e.g., speaking, chewing, and swallowing). Treatments for hyposalivation are currently limited to medications (e.g., the muscarinic receptor agonists pilocarpine and cevimeline) that induce saliva secretion from residual acinar cells and the use of saliva substitutes. However, given that these therapies provide only temporary relief, the development of alternative treatments to restore gland function is essential. Previous studies demonstrated that laminin 1 (L1) is critical for intact salivary cell cluster formation and organization. However, the full L1 sequence is not suitable for clinical applications, as each protein domain may contribute to unwanted effects, such as degradation, tumorigenesis, and immune responses that, when compounded, outweigh the potential benefits provided by their sum. Although the L1 peptides YIGSR and A99 linked to fibrin hydrogels (FHs) promote intact salivary epithelial formation in vitro, little is known about their role during salivary gland regeneration in vivo. Therefore, the goal of this study was to demonstrate whether L1 peptides conjugated to FHs promote tissue regeneration in a wound-healing model of mouse submandibular glands (mSMGs). Our results suggest that YIGSR-A99 peptides, chemically conjugated to FHs and applied to wounded mSMGs in vivo, formed new organized salivary tissue. In contrast, wounded mSMGs treated with FHs alone or in the absence of a scaffold showed disorganized collagen formation and poor tissue healing. Together these studies indicate that damaged salivary gland tissue can grow and differentiate when treated with FHs containing L1 peptides.

Keywords: biocompatible materials, bioengineering, extracellular matrix, laminin, saliva, wound healing

Introduction

Hyposalivation is associated with several conditions, including 1) Sjögren's syndrome, an autoimmune disease with a prevalence of 1% globally, and 2) γ-irradiation therapy, which is administered every year to approximately 60,000 head and neck cancer patients in the United States (Pillemer et al. 2001; Chambers et al. 2004). Treatments for hyposalivation are limited to medications (e.g., the muscarinic receptor agonists pilocarpine and cevimeline) that induce saliva secretion from residual acinar cells and the use of saliva substitutes, both of which provide only temporary relief (Villa et al. 2015). Given that these therapies target relatively surface-level symptoms, the development of alternative treatments to restore gland function is essential. Several alternative approaches to our modified fibrin hydrogel (FH) scaffold would seem to be logical candidates for restoring salivary gland (SG) function, such as the use of stem cells, embryonic organ culture transplantation, scaffolds other than FH, and transplantation of an artificial SG. Regarding stem cells, recent studies have shown that c-Kit$^+$ cells, which are normally expressed in very low amounts in SG specimens, can be expanded ex vivo to restore SG function (Nanduri et al. 2011; Nanduri et al. 2013). However, further characterization, such as identifying how they incorporate into host tissue, as well as what their long-term secondary effects are (e.g., tumorigenesis and survival rates), is required before translating this approach into humans. Regarding embryonic organ culture transplantation, previous studies have demonstrated that mouse embryonic salivary cells (i.e., submandibular, sublingual, and parotid gland cells) grown in an organ culture can be transplanted in vivo (Ogawa et al. 2013). However, a diminished gland size and a brief period of survival for animal subjects following treatment significantly decrease the utility of this model for human application. Regarding scaffolds other than FH, a host of new biomaterials (e.g., PLLA [poly-L-lactic acid], PLGA

[1]School of Dentistry, The University of Utah, Salt Lake City, UT, USA
[2]Department of Chemical and Biological Engineering, University at Buffalo, The State University of New York, Buffalo, NY, USA
[3]Department of Biomedical Engineering, School of Engineering and Applied Sciences, University at Buffalo, The State University of New York, Buffalo, NY, USA
[4]Center of Bioinformatics and Life Sciences, University at Buffalo, The State University of New York, Buffalo, NY, USA

A supplemental appendix to this article is available online.

Corresponding Author:
O.J. Baker, School of Dentistry, The University of Utah, Salt Lake City, UT 84108-1201, USA.
Email: olga.baker@hsc.utah.edu

[poly-L-lactic-co-glycolic acid], nanofibers, and chitosan) has been shown to allow cells to grow, attach to the scaffold, and organize to acquire features observed in native salivary epithelium (Aframian et al. 2000; Cantara et al. 2012; Soscia et al. 2013; Hsiao and Yang 2015; Yang and Hsiao 2015). Yet, further studies will be required to show their effects in vivo. Additionally, recent studies showed that human cells grown on a hyaluronic acid–based scaffold and transplanted into a wounded mouse parotid gland appeared to allow integration of the scaffold into the wound, with subsequent expression of markers of progenitor cells noted (Pradhan-Bhatt et al. 2014). But these results did not monitor scaffold degradation or evidence of new tissue formation in vivo, raising concerns with the stability of the biomaterial and capacity for regeneration, respectively. Finally, transplantation of an artificial SG remains an attractive option, albeit one in early stages of development. Therefore, engineering an environment that promotes functional SG regeneration in vivo would be a significant step forward in advancing the treatment of SG dysfunction.

FHs are water-swollen, cross-linked polymeric structures that form scaffolds and allow for 3-dimensional cell assembly. FHs are known to support cell infiltration and increase cell proliferation, while fibrin degradation products have no adverse effects on cell function or viability (Lei et al. 2009). Fibrin, a major protein component of blood clots, is able to form a gel at physiologic temperatures. It has been used extensively in biomedical engineering applications ranging from cardiovascular tissue engineering to wound-healing experiments (due to its biocompatibility and its ability to biodegrade in vivo; Yao et al. 2008; Slaughter et al. 2009). Previous studies demonstrated that rat parotid Par-C10 cells and freshly isolated mouse parotid cells are capable of forming 3-dimensional structures with lumens and apical tight junctions when grown on growth factor–reduced Matrigel (GFR-MG). Conversely, both Par-C10 and parotid gland cells grown on FH failed to develop completely, indicating that components present on GFR-MG may induce a degree of differentiation in parotid single cells. Following these studies, we decided to combine GFR-MG with FH in an attempt to recover acinar formation. Surprisingly, this combination did not result in a recovery of acinar formation for either Par-C10 or parotid gland cells, indicating that the acinar-inducing components of GFR-MG require critical concentrations of ≥1 biochemical factors to be functional. To determine what components of GFR-MG may be necessary for differentiation, we decided to incorporate into FHs 2 growth factors present in GFR-MG (i.e., EGF and IGF-1) that enhance salivary cell survival and differentiation. While these factors were not enough to induce acinar formation, they were able to induce amylase expression in parotid gland primary cells (McCall et al. 2013). More recently, we demonstrated that highly purified laminin 1 (L1) improved growth, organization, and differentiation of salivary cell clusters grown in vitro (Maruyama et al. 2015). Nonetheless, the full L1 sequence is not suitable for clinical applications, as each protein domain brings problems such as degradation, tumorigenesis, and immune responses that, when compounded, outweigh the potential benefits provided by their sum (Topley et al. 1993). Still, the benefits of L1 can be obtained while minimizing the risks by targeting select L1 peptides (L_{1p}) within the L1 sequence: 1) the A99 peptide corresponding to the α_1 chain from L1 (important for cell adhesion) and 2) the YIGSR peptide corresponding to the β_1 chain from L1 (also important for cell adhesion and migration; Hosokawa et al. 1999; Yamada et al. 2013). Recently, we created 3-dimensional salivary cell clusters using a modified FH matrix containing immobilized L_{1p} (L_{1p}-FH). Specifically, we reported that the YIGSR peptide improved morphology and lumen formation in rat parotid Par-C10 cells as compared with cells grown on unmodified FHs. Notably, when YIGSR was combined with the A99 peptide, we observed the formation of functional 3-dimensional salivary cell clusters with increased attachment and number of cell clusters. In summary, L_{1p}-FH supported attachment and differentiation of SG cell clusters with mature lumens. Therefore, the goal of this study was to demonstrate whether L_{1P}-FH is useful for promoting tissue regeneration in wounded mouse submandibular glands (mSMGs) in vivo.

Materials and Methods

Synthesis of L_{1p}, L_{1p}-Conjugated Fibrinogen, and DyLight 680–Conjugated Fibrinogen

The overall synthesis scheme of peptides, peptide-conjugated fibrinogen, and DyLight 680–conjugated fibrinogen is described in the Appendix.

FH Preparation

FHs were plated in 8-well chambers, as detailed in the Appendix.

Preparation of mSMG Cell Clusters

mSMG cells were dissociated, as seen in the Appendix.

Plating and Counting of mSMG Cell Clusters on FH or L_{1p}-FH

mSMG cell clusters were plated and counted after 6 d of growth, as outlined in the Appendix.

Surgical Procedure

An animal model for surgically wounded mSMGs was created (see Appendix). All animal usage, anesthesia, and surgery were conducted with the approval of The University of Utah Institutional Animal Care and Use Committee, in accordance with its strict guidelines.

Monitoring of Scaffold Stability

FHs were implanted and monitored in vivo with the Xenogen IVIS 100 Bioluminescent Imager at postsurgery days 3 and 8, as detailed in the Appendix.

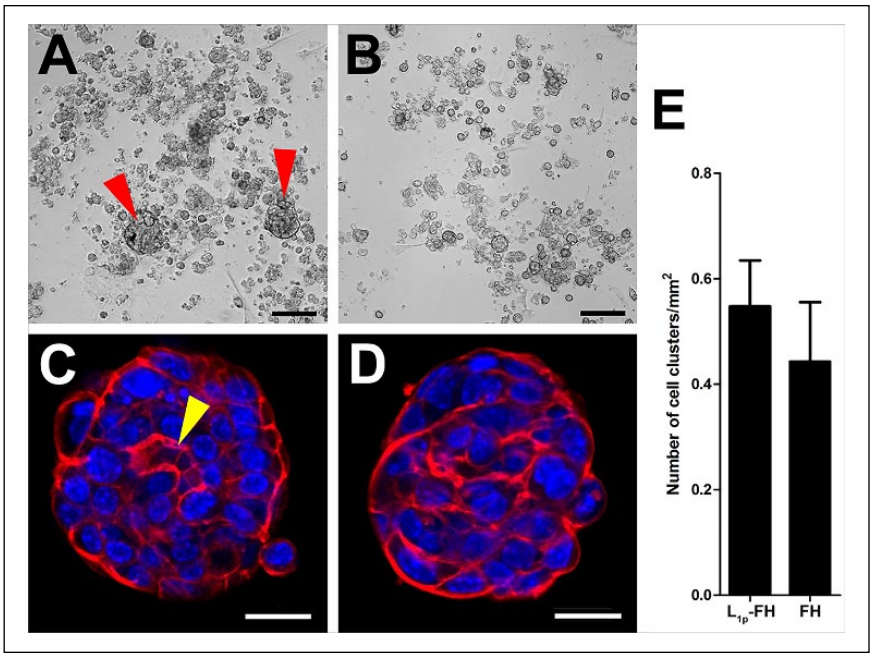

Figure 1. Mouse submandibular gland cell cluster organization on L_{1p}-FH (**A**, **C**) or FH (**B**, **D**). Images were taken with a EVOS XL Core with a 4× objective (A, B) or a confocal Zeiss LSM 700 microscope with 20× objective (C, D) to visualize cell cluster organization (red: F-actin, blue: nuclei). Scale bars represent 100 µm (A, B) and 20 µm (C, D). Mouse submandibular gland cell cluster formation per square millimeter was calculated (**E**). Red arrowheads indicate cell clusters, and yellow arrowhead indicates cell cluster lumen. FH, fibrin hydrogel; L_{1p}, laminin 1 peptides.

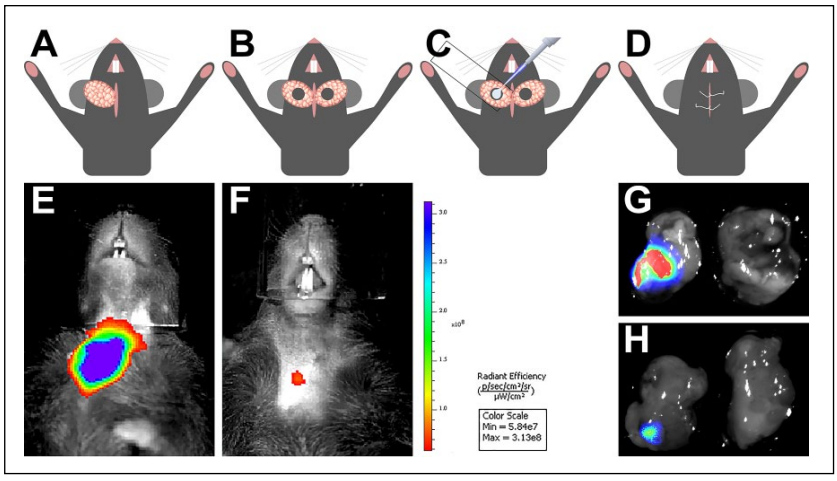

Figure 2. Surgical procedure to create wounded mouse submandibular glands (mSMGs) and monitor hydrogel stability in vivo. mSMGs were exposed, and a surgical wound was created on both glands with a 3-mm-diameter biopsy punch (**A, B**). Fibrin hydrogel scaffolds were injected into the surgical wound, where a coverslip was placed underneath to prevent leakage (**C**). The incision was closed with an interrupted 4-0 suture (**D**). Fibrin hydrogel stability was monitored in a Xenogen IVIS 100 Bioluminescent Imager at day 3 (**E**) and day 8 (**F**). mSMGs were dissected, and the fluorescence intensity was corroborated with a ChemiDoc System at day 3 (**G**) and day 8 (**H**). A total of 5 mice per group were tested.

Histologic Studies

Gland sections were stained with hematoxylin and eosin, Masson's trichrome, and picrosirius red stain, as well as immunostained for the indicated proteins (see Appendix).

Confocal Microscopy

mSMG cell clusters and tissue sections were analyzed with a confocal Zeiss LSM 700 microscope, as described in the Appendix.

Results

mSMG Cells Formed Organized Acinar Clusters When Grown on L_{1p}-FH

mSMG cell clusters were grown on L_{1p}-FH or FH for 6 d (Appendix Table 1). Our results showed that cells grown on L_{1p}-FH formed round salivary cell clusters (Fig. 1A, C; red arrowheads). In contrast, cells grown on FH formed fewer round cell clusters (Fig. 1B, D). L_{1p}-FH appeared to promote cell clustering over FH, as shown in Figure 1A, C, and E. To demonstrate formation of salivary lumens, mSMG cell clusters were stained with phalloidin to localize F-actin and TO-PRO-3 iodide as a nuclear marker. Interestingly, mSMG cells grown on L_{1p}-FH formed salivary cell clusters with an apical F-actin ring (Fig. 1C; yellow arrowhead), while cells grown on FH alone formed only some clusters, with most lacking lumens (Fig. 1D), suggesting that L_{1p} within FH promoted lumen formation.

L_{1p}-FH Were Successfully Implanted and Monitored In Vivo

mSMGs were exposed (Fig. 2A), and a surgical wound was created with a 3-mm diameter biopsy punch (Fig. 2B). To determine the effects of L_{1p}-FH on formation of new glandular tissue, we employed the dye-conjugated FH scaffold with or without L_{1p} (i.e., FH^{680} and L_{1p}-FH^{680}; Appendix Table 1) and compared them with a contralateral control with no scaffold (Fig. 2C). The skin incision was then sutured (Fig. 2D), and postsurgical studies (live animal imaging and mSMG histology) were performed. As shown in Figure 2, the fluorescence intensity of the hydrogels on day 8 was approximately 10 times lower as compared with that on postsurgery day 3 (Fig. 2E, F; Appendix Fig. 2), suggesting possible degradation of the FH scaffold over time in vivo. These results were corroborated by dissecting the

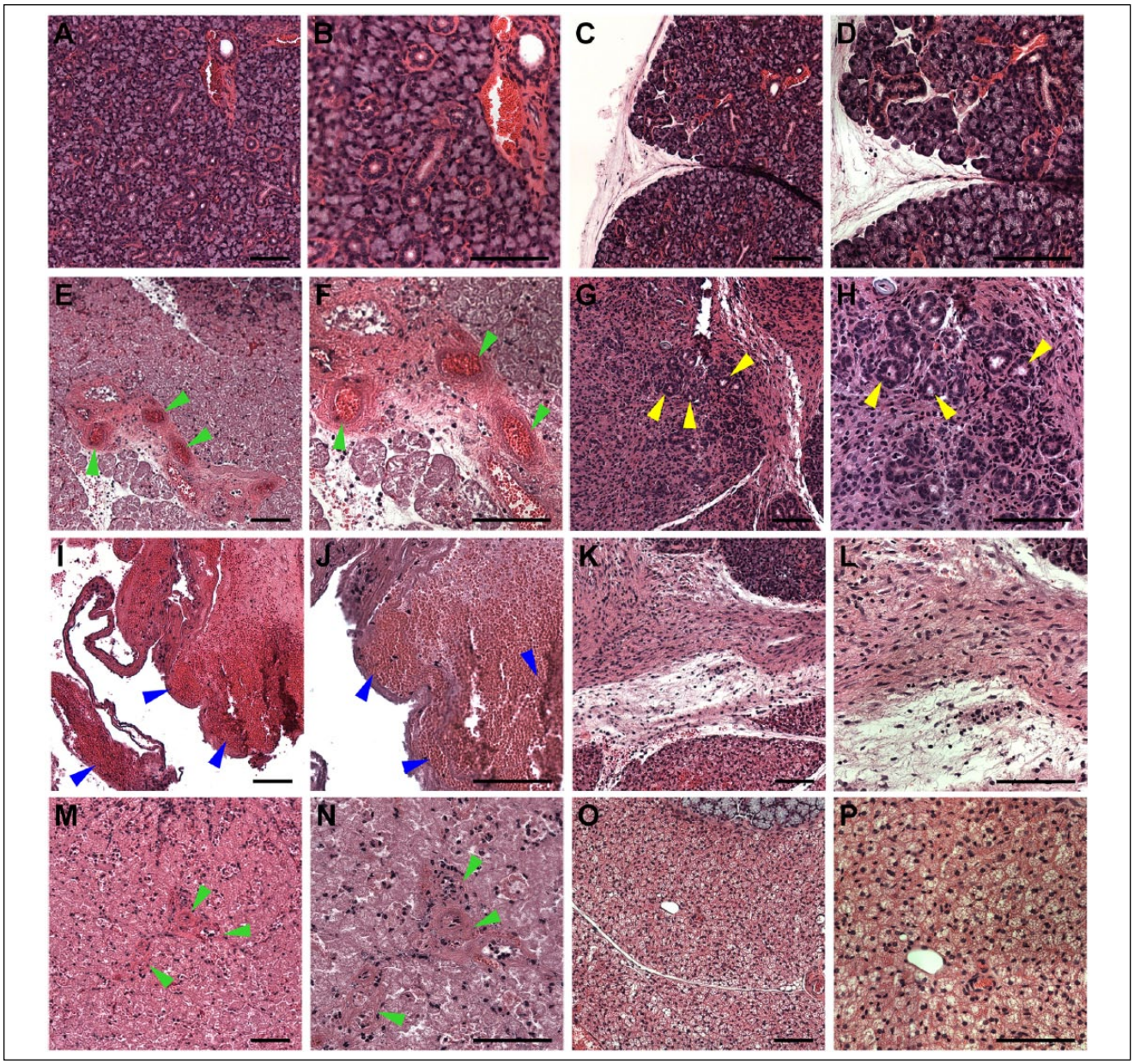

Figure 3. Hematoxylin and eosin–stained images of mouse submandibular glands (mSMGs) treated with and without fibrin hydrogel (FH) scaffolds (magnification 10× or 20× from Appendix Fig. 3; yellow boxes). Shown are native mSMGs (**A, B**: day 0), wounded mSMGs without scaffold (**C, D**: day 0), wounded mSMGs with dye-conjugated FH scaffold with laminin 1 peptide (DyLight 680; **E, F**: day 3; **G, H**: day 8), wounded mSMGs without scaffold (**I, J**: day 3; **K, L**: day 8), and wounded mSMGs with dye-conjugated FH scaffold (DyLight 680; **M, N**: day 3; **O, P**: day 8). Arrowheads indicate blood vessels (green), organized round structures with lumen (yellow), and blood clots (blue), respectively. Scale bars represent 100 µm. Representative image from a total of 5 mice per group.

glands and measuring the fluorescence signals in a Chemi-Doc MP imaging system. As shown in Figure 2 (G, day 3; H, day 8), both glands are visible with use of bright field. In contrast, only glands filled with L_{1p}-FH^{680} were visible under ultraviolet light (left glands).

L_{1p}-FH Induced Wound Healing In Vivo

To determine whether L_{1p}-FH^{680} promoted healing of mSMG surgical wounds in vivo, we stained the mSMG tissue sections with hematoxylin and eosin and compared the day 3 (Appendix Fig. 3C, E, G) and day 8 (Appendix Fig. 3D, F, H) samples to day 0 control samples (Appendix Fig. 3A, nonwounded; B, wounded). As shown in Appendix Figures 3 (C, G) and 4 (A, C), mSMG surgical wounds that were covered with L_{1p}-FH^{680} or FH^{680} displayed partial closure of the wound on day 3 post-surgery. In contrast, untreated wounds (no scaffold) displayed empty wounded spaces at postsurgery day 3 (Appendix Fig. 3E). Higher-magnification images revealed the presence of new blood vessels in wounds that were treated with L_{1p}-FH^{680}

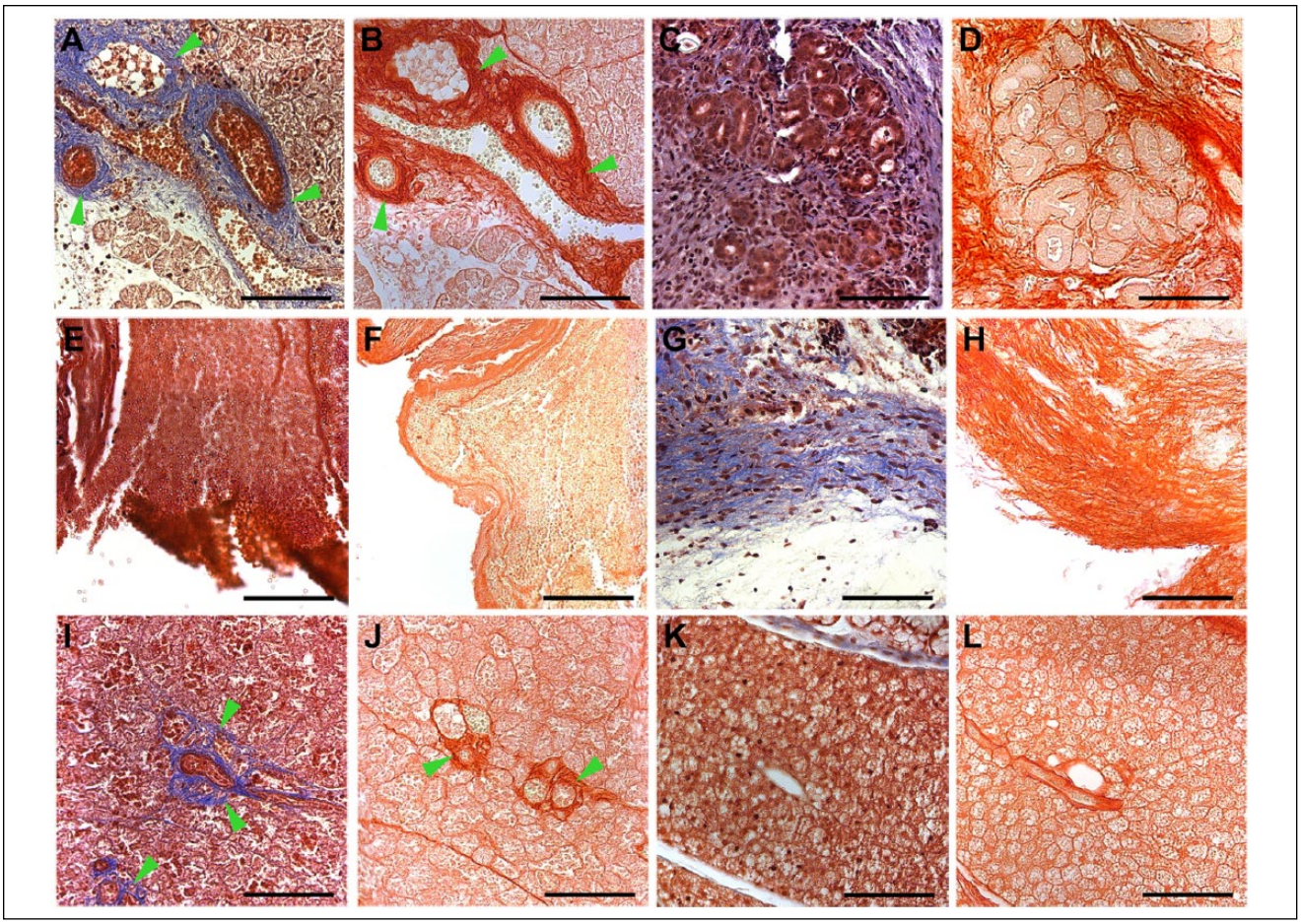

Figure 4. Stained images of mouse submandibular glands (mSMGs) treated with and without fibrin hydrogel (FH) scaffolds (magnification 20×): Masson's trichrome (**A**, **C**, **E**, **G**, **I**, **K**) and picrosirius red (**B**, **D**, **F**, **H**, **J**, **L**). Shown are wounded mSMGs with dye-conjugated FH scaffold with laminin 1 peptide (DyLight 680; A, B: day 3; C, D: day 8), wounded mSMGs without scaffold (E, F: day 3; G, H: day 8), and wounded mSMGs with dye-conjugated FH scaffold (DyLight 680; I, J: day 3: K, L: day 8). Scale bars represent 100 µm. Green arrowheads indicate collagen fibrils. Representative image from a total of 5 mice per group.

(Fig. 3E, F; green arrowheads) or FH^{680} (Fig. 3M, N; green arrowheads). In contrast, untreated wounds displayed blood clots at postsurgery day 3 (Fig. 3I, J; blue arrowheads).

On day 8 postsurgery, mSMG surgical wounds that were covered with L_{1p}-FH^{680} displayed almost complete wound closure (Fig. 4B; Appendix Fig. 3D). In contrast, untreated (Appendix Fig. 3F) or FH^{680}-treated (Fig. 4D; Appendix Fig. 3H) wounds exhibited signs of fibrosis and incomplete wound healing. In addition, L_{1p}-FH^{680}-treated wounds showed the presence of organized round structures with lumens indicative of acinar and ductal structures (Fig. 3G, H; yellow arrowheads). In contrast, untreated wounds (no scaffold) showed disorganized fibrotic tissue (Fig. 3K, L), while FH^{680}-treated wounds formed fibrotic tissues and failed to form organized round structures (Fig. 3O, P). In some instances, FH^{680}-treated wounds showed the presence of adipose tissue (Appendix Fig. 4D; green arrows). L_{1p}-FH^{680}-treated wounds also displayed a significantly higher number of Ki-67-positive cells as compared with controls, indicating promotion of cell proliferation (Appendix Fig. 5). Together, these results suggest that L_{1p}-FH^{680} is suitable for in vivo applications and accelerates wound healing in mSMGs as compared with no scaffold or FH alone.

L_{1p}-FH Induced Formation of Organized Conjunctive Tissue In Vivo

Next, we stained the mSMG tissue sections with Masson's trichrome and picrosirius red stains to examine formation of new conjunctive tissue. As shown in Figure 4, surgical wounds that were covered with L_{1p}-FH^{680} (Fig. 4A, B) or FH^{680} (Fig. 4I, J) formed organized collagen at postsurgery day 3 (see green arrowheads). In contrast, wounded mSMGs that were treated with no scaffold displayed poor collagen formation and empty spaces (Fig. 4E, F). On day 8 postsurgery, mSMG surgical wounds covered with L_{1p}-FH^{680} displayed organized round acinar and ductal structures (Fig. 4C, D). However, collagen staining was weak in areas of regenerated acinar-ductal structures, most likely because new blood vessel formation is no longer needed at this stage of tissue recovery. In contrast, wounded mSMGs that were treated with no scaffold formed only disorganized collagen (Fig. 4G, H). Likewise, wounded

mSMGs that were treated with FH^{680} failed to form organized round structures (Fig. 4K, L).

L_{1p}-FH Induced Formation of Salivary Epithelium In Vivo

To determine whether mSMG surgical wounds covered with L_{1p}-FH^{680} regenerated new salivary epithelium, we stained the mSMG sections with the apical tight junction marker zonula occludens 1 (ZO-1) and basolateral marker E-cadherin. As shown in Figure 5A and B, on postsurgery day 8, surgical wounds that were covered with L_{1p}-FH^{680} expressed apical ZO-1 (green) and basolateral E-cadherin (red), indicative of epithelial tissue formation. In contrast, untreated (Fig. 5G, H) or FH^{680}-treated (Fig. 5M, N) wounds displayed weak ZO-1 and E-cadherin staining, indicating poor epithelial formation (compare with unwounded areas; yellow-dotted area).

We also stained the mSMG tissue sections with markers of SG differentiation, including the water channel protein aquaporin 5 (AQP5), the apical chloride transporter TMEM16A, the basolateral Na^+/K^+-ATPase, and the ductal structure marker cytokeratin 7 (K7). Surprisingly, surgical wounds covered with L_{1p}-FH^{680} showed AQP5 (green) signal in some areas (Fig. 5E, F; see contrast with unwounded tissue; yellow-dotted area). Conversely, untreated (Fig. 5K, L) or FH^{680}-treated (Fig 5Q, R) wounds displayed no AQP5 (green) staining, indicating a lack of secretory epithelium in this area. Additionally, surgical wounds that were covered with L_{1p}-FH^{680} showed apical TMEM16A localization (green) and organized K7 signal (red; Fig. 5C, D), but untreated (Fig. 5I, J) or FH^{680}-treated (Fig. 5O, P) wounds displayed poor TMEM16A (green) and K7 (red) staining, again indicating a lack of secretory epithelium in this area (see the contrast with unwounded tissue; yellow-dotted area). Interestingly, L_{1p}-FH^{680}-treated wounds showed basolateral Na^+/K^+-ATPase localization (Fig. 5E, F; red), indicating functional epithelium. Once again, untreated (Fig. 5K, L) or FH^{680}-treated (Fig. 5Q, R) wounds did not display Na^+/K^+-ATPase staining, indicating poor epithelial formation (see the contrast with unwounded areas; yellow-dotted area).

Discussion

Integrins link cells to the extracellular matrix, supporting cell migration, proliferation, and long-term viability (Cattavarayane et al. 2015). The YIGSR and A99 peptides likely bind to several integrins, including $\alpha_3\beta_1$, $\alpha_4\beta_1$, and $\alpha_6\beta_1$, promoting cell migration, proliferation, and cell adhesion (Maeda et al. 1994; Frith et al. 2012). Previous studies indicated that Par-C10 cells grown on combinations of L_{1p} (i.e., YIGSR and A99) linked to FH (L_{1p}-FH) improved cell migration, proliferation, and adhesion (Nam et al. 2016). Likewise, in the current study, freshly isolated mSMG cells grown on L_{1p}-FH also showed improved cell migration, proliferation, and adhesion (Fig. 1). Interestingly, L_{1p}-FH promoted SG regeneration in an in vivo wound-healing mSMG model. The main advantage of this model over an irradiated model is that the wound size is controlled, thereby enabling direct monitoring of wound regeneration as well as the fate of the scaffold over time. Our results are consistent with our previous studies with SG cell clusters in vitro (Maruyama et al. 2015; Nam et al. 2016). Notably, this is the first study showing these effects in SGs in vivo; therefore, the mechanism of gland regeneration is not fully understood. Collagen organization plays a critical role in the quality of the wound (Ehrlich and Hunt 2012). Our results indicate that L_{1p}-FH^{680} is able to promote organized collagen formation (Fig. 4C, D). Additionally, L_{1p}-FH^{680} likely attracts functional cells to the wounded site, as previous studies have demonstrated that L1 promotes activation of muscle and cardiac regeneration (Riederer et al. 2015; Peña et al. 2016). Alternatively, we speculate that L_{1p} conjugated to FH could have activated resident stem and progenitor cells that contributed to gland homeostasis through interactions with specific integrins (Imhof and Aurrand-Lions 2004; Riopel et al. 2013). More studies may be required to examine how L_{1p}-FH-promoted gland regeneration in vivo.

Regarding the expression of functional markers, we found that the apical Ca^{2+}-activated chloride channel TMEM16A was expressed in regenerating mSMGs covered with L_{1p}-FH (Fig. 5C, D; green). This channel is important for saliva secretion, as previous studies demonstrated that its knockdown reduced saliva production in mice (Yang et al. 2008). We also detected basolateral expression of Na^+/K^+-ATPase in the regenerating glands (Fig. 5E, F; red). Na^+/K^+-ATPase maintains a Na^+ gradient toward the intracellular space by exporting $3Na^+$ and importing $2K^+$ per ATP molecule hydrolyzed. Along with Nkcc1, Na^+/K^+-ATPase maintains a higher concentration of Cl^- inside the cells, countering the cation imbalance created by Na^+. This high intracellular Cl^- concentration is critical for primary saliva secretion (Catalan et al. 2009). Finally, we detected a weak AQP5 signal in the regenerating glands (Fig. 5E, F; green). AQP5 is an apical protein mostly expressed in acinar cells that induces water transport across the cell membrane during fluid secretion (Matsuzaki et al. 1999; Matsuzaki et al. 2012). The weak AQP5 signal observed in this study could be attributed to the time of regeneration. Specifically, previous studies demonstrated that AQP5 expression in mice increases as the animal develops (Aure et al. 2011). Therefore, we speculate that AQP5 will appear at later stages of gland regeneration. Future studies will be necessary to confirm this hypothesis.

Regarding the structural proteins TJ protein ZO-1 (membrane-anchored scaffolding protein) and basolateral E-cadherin (type 1 transmembrane protein), we found that both molecules were expressed in the regenerating SGs (Fig. 5A, B). While ZO-1 serves as barrier between the extracellular environment and the glandular lumen to allow polarized saliva secretion, E-cadherin is important for cell-cell adhesion (Walker et al. 2008; Baker 2016). We also found organized ductal structures (K7) in the regenerating SGs (Fig. 5C, D; red). The expression of these structural proteins indicates that the regenerating tissue exhibits epithelial integrity.

An important aspect of this study is that FH of human origin can be successfully used in mice with no rejection by the host,

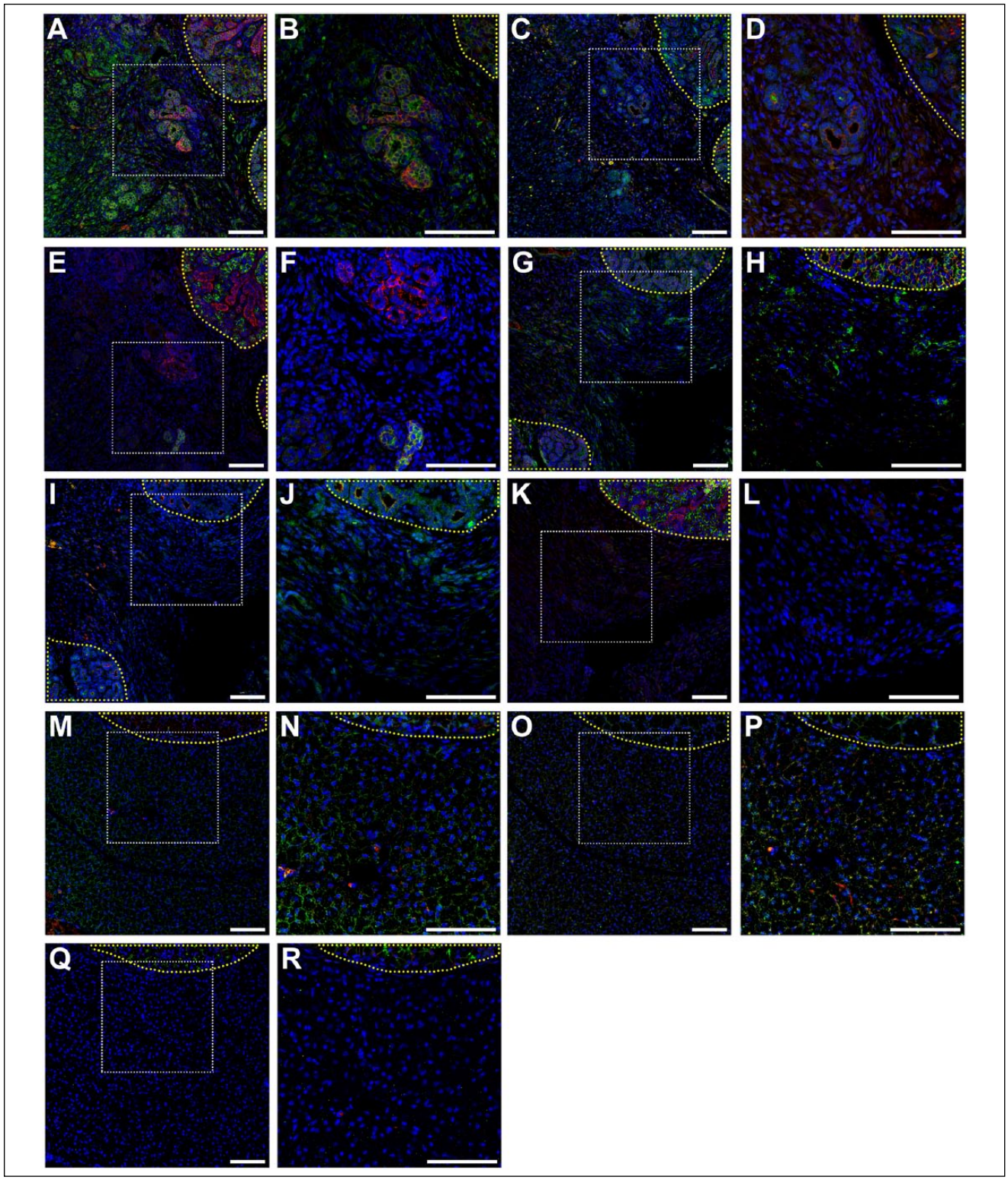

Figure 5. Salivary structural and functional marker organization in wounded mouse submandibular glands (mSMGs) with dye-conjugated fibrin hydrogel (FH) scaffold with laminin 1 peptide (DyLight 680; **A–F**), wounded mSMGs without scaffold (**G–L**), and wounded mSMGs with dye-conjugated FH scaffold (DyLight 680; **M–R**) was determined with confocal microscopy (magnification 10x or 20x from white dotted areas) as follows: zonula occludens 1 (green; A, B, G, H, M, N), E-cadherin (red; A, B, G, H, M, N), TMEM16A (green; C, D, I, J, O, P), cytokeratin 7 (red; C, D, I, J, O, P), aquaporin 5 (green; E, F, K, L, Q, R), Na^+/K^+-ATPase (red; E, F, K, L, Q, R), and TO-PRO-3 (blue; everywhere). Yellow-dotted areas are unwounded areas. Scale bars represent 100 μm. Representative image from a total of 5 mice per group.

consistent with previous studies using this scaffold in a variety of systems (Janmey et al. 2009). This is a benefit for future translational studies, as the scaffold will not cause host rejection when used for SG regeneration. This is important, as tissue repair involves a complex inflammatory response characterized by the recruitment, proliferation, and activation of immune cells such as neutrophils, macrophages, natural killer cells, as well as B cells and T cells (Wynn and Vannella 2016). Finally, the fluorescence intensity of FH decreased 10-fold over a period of 8 d (Fig. 2E–H; Appendix Fig. 2), indicating that cells were able to degrade the FH and repopulate the gland at this time (after modified FH elicited its actions). These results are consistent with previous studies showing that FH can be easily degraded in vivo (Jockenhoevel et al. 2001; Li et al. 2015). This is important because FH can be successfully used as a delivery system in SGs.

In summary, we demonstrated the ability of an FH modified with L_{1p} (L_{1p}-FH) to form new and functional SG tissue. Our results suggest that L_{1p}-FH is suitable for in vivo applications, as it is both biodegradable and biocompatible and it significantly accelerates formation of new tissue as compared with FH alone or no scaffold. The newly formed gland tissues displayed organized acinar and ductal cell organization. These results suggest that L_{1p}-FH may have activated multiple cellular processes that contributed to tissue regeneration. Long-term studies will address the function of regenerated glands.

Author Contributions

K. Nam, contributed to conception, design, data acquisition, analysis, and interpretation, drafted and critically revised the manuscript; C.-S. Wang, C.L.M. Maruyama, contributed to conception, design, data acquisition, and analysis, drafted the manuscript; P. Lei, S.T. Andreadis, contributed to conception and data interpretation, critically revised the manuscript; O.J. Baker, contributed to conception, design, and data acquisition, interpretation, drafted and critically revised the manuscript. All authors gave final approval and agree to be accountable for all aspects of the work.

Acknowledgments

This work was supported by the National Institutes of Health (DE021697 and DE022971). The authors thank Chieh-Hsiang Yang (Department of Bioengineering, University of Utah) for his assistance in performing the animal experiments. The authors declare no potential conflicts of interest with respect to the authorship and/or publication of this article.

References

Aframian DJ, Cukierman E, Nikolovski J, Mooney DJ, Yamada KM, Baum BJ. 2000. The growth and morphological behavior of salivary epithelial cells on matrix protein-coated biodegradable substrata. Tissue Eng. 6(3):209–216.

Aure MH, Larsen HS, Ruus AK, Galtung HK. 2011. Aquaporin 5 distribution pattern during development of the mouse sublingual salivary gland. J Mol Histol. 42(5):401–408.

Baker OJ. 2016. Current trends in salivary gland tight junctions. Tissue Barriers. 4(3):e1162348.

Cantara SI, Soscia DA, Sequeira SJ, Jean-Gilles RP, Castracane J, Larsen M. 2012. Selective functionalization of nanofiber scaffolds to regulate salivary gland epithelial cell proliferation and polarity. Biomaterials. 33(33):8372–8382.

Catalan MA, Nakamoto T, Melvin JE. 2009. The salivary gland fluid secretion mechanism. J Med Invest. 56 Suppl:192–196.

Cattavarayane S, Palovuori R, Tanjore Ramanathan J, Manninen A. 2015. A6β1- and αv-integrins are required for long-term self-renewal of murine embryonic stem cells in the absence of LIF. BMC Cell Biol. 16:3.

Chambers MS, Garden AS, Kies MS, Martin JW. 2004. Radiation-induced xerostomia in patients with head and neck cancer: pathogenesis, impact on quality of life, and management. Head Neck. 26(9):796–807.

Ehrlich HP, Hunt TK. 2012. Collagen organization critical role in wound contraction. Adv Wound Care (New Rochelle). 1(1):3–9.

Frith JE, Mills RJ, Hudson JE, Cooper-White JJ. 2012. Tailored integrin–extracellular matrix interactions to direct human mesenchymal stem cell differentiation. Stem Cells Dev. 21(13):2442–2456.

Hosokawa Y, Takahashi Y, Kadoya Y, Yamashina S, Nomizu M, Yamada Y, Nogawa H. 1999. Significant role of laminin-1 in branching morphogenesis of mouse salivary epithelium cultured in basement membrane matrix. Dev Growth Differ. 41(2):207–216.

Hsiao YC, Yang TL. 2015. Data supporting chitosan facilitates structure formation of the salivary gland by regulating the basement membrane components. Data Brief. 4:551–558.

Imhof BA, Aurrand-Lions M. 2004. Adhesion mechanisms regulating the migration of monocytes. Nat Rev Immunol. 4(6):432–444.

Janmey PA, Winer JP, Weisel JW. 2009. Fibrin gels and their clinical and bioengineering applications. J R Soc Interface. 6(30):1–10.

Jockenhoevel S, Zund G, Hoerstrup SP, Chalabi K, Sachweh JS, Demircan L, Messmer BJ, Turina M. 2001. Fibrin gel: advantages of a new scaffold in cardiovascular tissue engineering. Eur J Cardiothorac Surg. 19(4):424–430.

Lei P, Padmashali R, Andreadis ST. 2009. Cell-controlled and spatially arrayed gene delivery from fibrin hydrogels. Biomaterials. 30(22):3790–3799.

Li Y, Meng H, Liu Y, Lee BP. 2015. Fibrin gel as an injectable biodegradable scaffold and cell carrier for tissue engineering. Scientific World J. 2015:685690.

Maeda T, Titani K, Sekiguchi K. 1994. Cell-adhesive activity and receptor-binding specificity of the laminin-derived yigsr sequence grafted onto staphylococcal protein a. J Biochem. 115(2):182–189.

Maruyama CL, Leigh NJ, Nelson JW, McCall AD, Mellas RE, Lei P, Andreadis ST, Baker OJ. 2015. Stem cell-soluble signals enhance multilumen formation in smg cell clusters. J Dent Res. 94(11):1610–1617.

Matsuzaki T, Susa T, Shimizu K, Sawai N, Suzuki T, Aoki T, Yokoo S, Takata K. 2012. Function of the membrane water channel aquaporin-5 in the salivary gland. Acta Histochem Cytochem. 45(5):251–259.

Matsuzaki T, Suzuki T, Koyama H, Tanaka S, Takata K. 1999. Aquaporin-5 (AQP5), a water channel protein, in the rat salivary and lacrimal glands: immunolocalization and effect of secretory stimulation. Cell Tissue Res. 295(3):513–521.

McCall AD, Nelson JW, Leigh NJ, Duffey ME, Lei P, Andreadis ST, Baker OJ. 2013. Growth factors polymerized within fibrin hydrogel promote amylase production in parotid cells. Tissue Eng Part A. 19(19–20):2215–2225.

Nam K, Jones JP, Lei P, Andreadis ST, Baker OJ. 2016. Laminin-111 peptides conjugated to fibrin hydrogels promote formation of lumen containing parotid gland cell clusters. Biomacromolecules. 17(6):2293–2301.

Nanduri LS, Lombaert IM, van der Zwaag M, Faber H, Brunsting JF, van Os RP, Coppes RP. 2013. Salisphere derived c-Kit+ cell transplantation restores tissue homeostasis in irradiated salivary gland. Radiother Oncol. 108(3):458–463.

Nanduri LS, Maimets M, Pringle SA, van der Zwaag M, van Os RP, Coppes RP. 2011. Regeneration of irradiated salivary glands with stem cell marker expressing cells. Radiother Oncol. 99(3):367–372.

Ogawa M, Oshima M, Imamura A, Sekine Y, Ishida K, Yamashita K, Nakajima K, Hirayama M, Tachikawa T, Tsuji T. 2013. Functional salivary gland regeneration by transplantation of a bioengineered organ germ. Nat Commun. 4:2498.

Peña B, Martinelli V, Jeong M, Bosi S, Lapasin R, Taylor MR, Long CS, Shandas R, Park D, Mestroni L. 2016. Biomimetic polymers for cardiac tissue engineering. Biomacromolecules. 17(5):1593–1601.

Pillemer SR, Matteson EL, Jacobsson LT, Martens PB, Melton LJ 3rd, O'Fallon WM, Fox PC. 2001. Incidence of physician-diagnosed primary Sjögren syndrome in residents of Olmsted County, Minnesota. Mayo Clin Proc. 76(6):593–599.

Pradhan-Bhatt S, Harrington DA, Duncan RL, Farach-Carson MC, Jia X, Witt RL. 2014. A novel in vivo model for evaluating functional restoration of a tissue-engineered salivary gland. Laryngoscope. 124(2):456–461.

Riederer I, Bonomo AC, Mouly V, Savino W. 2015. Laminin therapy for the promotion of muscle regeneration. FEBS Lett. 589(22):3449–3453.

Riopel MM, Li J, Liu S, Leask A, Wang R. 2013. Beta1 integrin-extracellular matrix interactions are essential for maintaining exocrine pancreas architecture and function. Lab Invest. 93(1):31–40.

Slaughter BV, Khurshid SS, Fisher OZ, Khademhosseini A, Peppas NA. 2009. Hydrogels in regenerative medicine. Adv Mater. 21(32–33):3307–3329.

Soscia DA, Sequeira SJ, Schramm RA, Jayarathanam K, Cantara SI, Larsen M, Castracane J. 2013. Salivary gland cell differentiation and organization on micropatterned PLGA nanofiber craters. Biomaterials. 34(28):6773–6784.

Topley P, Jenkins DC, Jessup EA, Stables JN. 1993. Effect of reconstituted basement membrane components on the growth of a panel of human tumour cell lines in nude mice. Br J Cancer. 67(5):953–958.

Villa A, Connell CL, Abati S. 2015. Diagnosis and management of xerostomia and hyposalivation. Ther Clin Risk Manag. 11:45–51.

Walker JL, Menko AS, Khalil S, Rebustini I, Hoffman MP, Kreidberg JA, Kukuruzinska MA. 2008. Diverse roles of E-cadherin in the morphogenesis of the submandibular gland: insights into the formation of acinar and ductal structures. Dev Dyn. 237(11):3128–3141.

Wynn TA, Vannella KM. 2016. Macrophages in tissue repair, regeneration, and fibrosis. Immunity. 44(3):450–462.

Yamada Y, Hozumi K, Katagiri F, Kikkawa Y, Nomizu M. 2013. Laminin-111-derived peptide-hyaluronate hydrogels as a synthetic basement membrane. Biomaterials. 34(28):6539–6547.

Yang TL, Hsiao YC. 2015. Chitosan facilitates structure formation of the salivary gland by regulating the basement membrane components. Biomaterials. 66:29–40.

Yang YD, Cho H, Koo JY, Tak MH, Cho Y, Shim WS, Park SP, Lee J, Lee B, Kim BM, et al. 2008. TMEM16A confers receptor-activated calcium-dependent chloride conductance. Nature. 455(7217):1210–1215.

Yao L, Liu J, Andreadis ST. 2008. Composite fibrin scaffolds increase mechanical strength and preserve contractility of tissue engineered blood vessels. Pharm Res. 25(5):1212–1221.